

Dynamics of pulsating swarmalators on a ring

Samali Ghosh,¹ Kevin O’Keeffe,² Gourab Kumar Sar,¹ and Dibakar Ghosh^{1,*}

¹*Physics and Applied Mathematics Unit, Indian Statistical Institute, 203 B. T. Road, Kolkata 700108, India*

²*Starling Research Institute, Seattle, USA*

(Received XX MONTH XX; accepted XX MONTH XX; published XX MONTH XX)

We study a simple one-dimensional model of swarmalators, a generalization of phase oscillators that swarm around in space as well as synchronize internal oscillations in time. Previous studies of the model focused on Kuramoto-type couplings, where the phase interactions are governed by phase *differences*. Here we consider Winfree-type coupling, where the interactions are *multiplicative*, determined by the product of a phase response function $R(\theta)$ and phase pulse function $P(\theta)$. This more general interaction (from which the Kuramoto phase differences emerge after averaging) produces rich physics: six long-term modes of organization are found, which we characterize numerically and analytically.

DOI: XXXXXXXX

I. INTRODUCTION

An interplay between synchronization [1–5] (self-organization in time) and swarming [6–9] (self-coordination in position) arises all over nature and technology, from biological microswimmers [10, 11] and colloidal motors [12, 13] to magnetic domain walls [14] and robotic swarms [15–17]. Tanaka *et al.* [18–20] gave one of the first mathematical treatments of this dual kind of pattern formation by introducing a universal model of chemotactic oscillators, oscillators that are pushed around by chemical gradients that, in turn, influence the oscillators’ phases. Later O’Keeffe *et al.* [21] introduced a generalized Kuramoto model of swarming oscillators or “swarmalators” leading to a new wave of work on swarmalation [22–37].

In most – if not all – of the studies above, the phase dynamics have ‘Kuramoto form’, by which we mean the phase dynamics $\dot{\theta}_i$ contain a sum over the sinusoid of the phase differences $N^{-1} \sum_j \sin(\theta_j - \theta_i)$ (usually with some spatial kernel $K(x_j - x_i)$). Yet this type of coupling, which defines the Kuramoto model [38], is actually an approximation of a more general type of Winfree coupling defined by: $\dot{\theta}_i = \sum_j R(\theta_i)P(\theta_j)$ [1]. Here, each of the j oscillators fires a pulse defined by the function $P(\theta)$, which is received by the i -th oscillator according to $R(\theta)$. This pulsatile coupling is present in many real-world systems, such as fireflies and heart cells, but has not yet been studied by the swarmalator community. This paper fills in this gap. As we show, it gives rise to several new states not seen in swarmalator models with regular Kuramoto-type coupling.

II. MODEL

The original swarmalator model concerned particles free to move in the plane [21]. It is, however, rather difficult to analyze [39], so instead researchers have turned to using the simpler *one dimensional swarmalator model* [23] where the swarmalators movements are confined to a 1d ring $x_i \in \mathbb{S}^1$. This model is

$$\dot{x}_i = v_i + \frac{J}{N} \sum_{j=1}^N \sin(x_j - x_i) \cos(\theta_j - \theta_i), \quad (1)$$

$$\dot{\theta}_i = \omega_i + \frac{K}{N} \sum_{j=1}^N \sin(\theta_j - \theta_i) \cos(x_j - x_i), \quad (2)$$

where (v_i, ω_i) are the natural velocities and frequencies and (J, K) are the associated coupling constants. The space dynamics in Eq. 1 describe the phase-dependent aggregation, while the phase dynamics in Eq. 2 capture position-dependent synchronization. This symmetry makes the model one of the few models of mobile oscillators that is tractable [40–42]. It has enabled exact analyses of swarmalators with distributed coupling [25, 43], phase frustration [44], random pinning [24, 45, 46], periodic forcing [47], multi-body interactions [48], noise [27], and low range coupling [49].

Here we swap the Kuramoto coupling for Winfree coupling $\sin(\theta_j - \theta_i) \rightarrow R(\theta_i)P(\theta_j)$. We leave the spatial dynamics the same. The model we thus study is

$$\dot{x}_i = v_i + \frac{J}{N} \sum_{j=1}^N \sin(x_j - x_i) \cos(\theta_j - \theta_i), \quad (3)$$

$$\dot{\theta}_i = \omega_i + \frac{K}{N} \sum_{j=1}^N R(\theta_i)P(\theta_j) \cos(x_j - x_i), \quad (4)$$

for $i = 1, \dots, N$, where $N \gg 1$. For simplicity, we work with swarmalators that have zero frequencies and

* dibakar@isical.ac.in

velocities, i.e., $\omega_i = 0 = v_i$ for all i . Following previous studies [50], we make the following choices for the pulse and response functions

$$P(\theta) = 1 + \cos \theta, \quad (5)$$

$$R(\theta) = -\sin \theta. \quad (6)$$

Next, we define the order parameters,

$$R_{x(\theta)} = r_{x(\theta)} e^{\iota \psi_{x(\theta)}} = \frac{1}{N} \sum_{j=1}^N e^{\iota x_j(\theta_j)}, \quad \iota = \sqrt{-1} \quad (7)$$

where $R_{x(\theta)}$ measures the amount of synchrony among swarmalators' positions and their phases. r_x and r_θ lie between 0 and 1 by definition, indicating the overall synchrony among the swarmalators' positions and their phases, respectively. ψ_x and ψ_θ are the mean position and phase of the overall population. We also define

$$W_\pm = S_\pm e^{\iota \phi_\pm} = \frac{1}{N} \sum_{j=1}^N e^{\iota(x_j \pm \theta_j)}, \quad (8)$$

where W_\pm measures the correlation between swarmalators' phases θ_j and their spatial angle x_j . We take the maximum of S_\pm and define $S = \max\{S_+, S_-\}$. Another order parameter denoted by $R_{2x(\theta)}$ is defined as,

$$R_{2x(\theta)} = r_{2x(\theta)} e^{\iota \psi_{2x(\theta)}} = \frac{1}{N} \sum_{j=1}^N e^{2\iota x_j(\theta_j)}, \quad (9)$$

which is beneficial to investigate the antiphase synchrony, where a phase difference of π is noticed among the swarmalators' phases. When antiphase synchrony is observed, then $r_{2x(\theta)} = 1$ but $r_{x(\theta)} \neq 1$.

These order parameters appear naturally in the equations of motion. Converting the trigonometric functions into complex exponentials, we can rewrite Eqs. (3) and (4) as,

$$\dot{x}_i = \frac{J}{2} \left[S_+ \sin(\phi_+ - (x_i + \theta_i)) + S_- \sin(\phi_- - (x_i - \theta_i)) \right], \quad (10)$$

$$\begin{aligned} \dot{\theta}_i = & -\frac{K}{4} \left[S_+ \sin(\phi_+ - (x_i - \theta_i)) - S_+ \sin(\phi_+ - (x_i + \theta_i)) \right. \\ & \left. + S_- \sin(\phi_- - (x_i - \theta_i)) - S_- \sin(\phi_- - (x_i + \theta_i)) \right] \\ & - \frac{K}{2} r_x \left[\sin(\psi_x - (x_i - \theta_i)) - \sin(\psi_x - (x_i + \theta_i)) \right]. \end{aligned} \quad (11)$$

We define $\xi_i = x_i + \theta_i$ and $\eta_i = x_i - \theta_i$ which leads

to

$$\begin{aligned} \dot{\xi}_i = & -\frac{K}{2} r_x (\sin(\psi_x - \eta_i) - \sin(\psi_x - \xi_i)) + \frac{1}{N} \left(\frac{J}{2} + \frac{K}{4} \right) \\ & \sum_{j=1}^N \sin(\xi_j - \xi_i) + \frac{1}{N} \left(\frac{J}{2} - \frac{K}{4} \right) \sum_{j=1}^N \sin(\eta_j - \eta_i) \\ & - \frac{K}{4N} \sum_{j=1}^N (\sin(\xi_j - \eta_i) - \sin(\eta_j - \xi_i)), \end{aligned} \quad (12)$$

$$\begin{aligned} \dot{\eta}_i = & \frac{K}{2} r_x (\sin(\psi_x - \eta_i) - \sin(\psi_x - \xi_i)) + \frac{1}{N} \left(\frac{J}{2} + \frac{K}{4} \right) \\ & \sum_{j=1}^N \sin(\eta_j - \eta_i) + \frac{1}{N} \left(\frac{J}{2} - \frac{K}{4} \right) \sum_{j=1}^N \sin(\xi_j - \xi_i) \\ & + \frac{K}{4N} \sum_{j=1}^N (\sin(\xi_j - \eta_i) - \sin(\eta_j - \xi_i)). \end{aligned} \quad (13)$$

Simplifying Eq. (12) and Eq. (13), we get,

$$\begin{aligned} \dot{\xi}_i = & -\frac{K}{2} r_x (\sin(\psi_x - \eta_i) - \sin(\psi_x - \xi_i)) + S_+ \left(\frac{J}{2} + \frac{K}{4} \right) \\ & \sin(\phi_+ - \xi_i) + S_- \left(\frac{J}{2} - \frac{K}{4} \right) \sin(\phi_- - \eta_i) \\ & - \frac{K}{4} (S_+ \sin(\phi_+ - \eta_i) - S_- \sin(\phi_- - \xi_i)), \end{aligned} \quad (14)$$

$$\begin{aligned} \dot{\eta}_i = & \frac{K}{2} r_x (\sin(\psi_x - \eta_i) - \sin(\psi_x - \xi_i)) + S_- \left(\frac{J}{2} + \frac{K}{4} \right) \\ & \sin(\phi_- - \eta_i) + S_+ \left(\frac{J}{2} - \frac{K}{4} \right) \sin(\phi_+ - \xi_i) \\ & + \frac{K}{4} (S_+ \sin(\phi_+ - \eta_i) - S_- \sin(\phi_- - \xi_i)), \end{aligned} \quad (15)$$

which contain S_\pm , $r_{x(\theta)}$ etc., as claimed.

III. RESULTS

A. Collective states

Next, we explore how our model behaves as the two parameters (J, K) are varied. We drew the phases and positions of $N = 10^3$ swarmalators uniformly at random from $[-\pi, \pi]$, then integrated the governing equations using Heun's method. We found the system always settles into six collective states depicted in Fig. 1 by varying J and K . These collective states are characterized through the order parameters by simultaneously varying J and K as shown in Fig. 2.

Static async: The swarmalators are distributed on the ring in such a way that their positions are static, but their phases evolve asynchronously over time, as shown

in Fig. 1(a). This state exists for negative J regardless of the value of K . Notice Fig. 2(a)-(d), $S_{\pm} = 0$ and $r_{2x(\theta)} = 0$ for this state.

Static π : The swarmalators synchronize into two distinct groups, one group is fully synchronized with (x^*, θ^*) and the other is synchronized exactly π units away $(x^* + \pi, \theta^* + \pi)$ (see Fig. 1(d)). We found that this state exists for $J, K > 0$. We observe $S_{\pm} = 1$ and $r_{2x(\theta)} = 1$ for this state (see Fig. 2(a)-(d)).

Static phase wave: Swarmalators form a phase wave that wraps around the circular domain once $x_i \pm \theta_i + C$ (notice Fig. 1(e)). The wave can go both clockwise and counterclockwise. In the coordinates (ξ_i, η_i) , ξ_i is splayed ($\xi_i = \frac{2\pi i}{N}$) and η_i is locked ($\eta_i = C$) or vice versa. The order parameters are $(S_+, S_-) = (1, 0)$ or vice versa, depending on whether the phase gradient of the rainbow is clockwise or anticlockwise, and $r_{2x(\theta)} \sim 0$ for this state (look Fig. 2(a)-(d)). This state exists only in the special case where the phase dynamics are turned off, $K = 0$ (and $J > 0$).

θ antiphase sync: The swarmalators are uniformly distributed along the run. Despite being evenly distributed in space, they organize their phase by separating into two distinct clusters, maintaining a phase difference of π . Figure 1(c) provides a snapshot of this state at a specific time. This state emerges in the region where $J = 0$ for any positive value of K . Figure 2(a)-(d) illustrate the order parameters for this state where, $S_{\pm} \approx 0.64$, r_{2x} is on the order of 10^{-2} , and $r_{2\theta} \sim 1$.

x anti-phase sync: We observe that the swarmalators positionally form two clusters at π difference and their phases are not completely disordered; rather, they are clustered around two points at π difference. Figure 1(f) best illustrates this state. We observe this state in regions $J > 0$ and $K < 0$. For this state, $S_{\pm} \approx 0.8 \pm 0.05$, $\frac{S_+}{S_-} \sim 1$, $r_{2x} = 1$, and $r_{2\theta} \approx 0.5$ which are depicted in Fig. 2(a)-(d).

Intermediate mixed state: This state is an intermediate state between the static async state and the θ antiphase sync state. Here, the swarmalators are randomly distributed in terms of position (Fig. 1(b)). However, when examining their internal dynamics, they are neither fully desynchronized nor organized into distinct clusters with a phase difference of π . Look at Fig. 2(a)-(d), where $S_{\pm} = 0$, r_{2x} in the order of 10^{-2} , and $0 < r_{2\theta} < 1$ in this state.

B. Analysis

1. Stability of the static π state

We analyze the stability of this state by simplifying around the equilibrium point in (ξ, η) space. Here, the swarmalators maintain a phase difference of π in both position and phase. Therefore, $r_x = 0$. For this, we first calculate the eigenvalues of the Jacobian matrix M ,

$$M = \begin{bmatrix} Z_{\xi} & Z_{\eta} \\ N_{\xi} & N_{\eta} \end{bmatrix}_{2N \times 2N} \quad (16)$$

where $(Z_{\xi})_{ij} = \frac{\partial \dot{\xi}_i}{\partial \xi_j}$, $(N_{\eta})_{ij} = \frac{\partial \dot{\eta}_i}{\partial \eta_j}$, $(Z_{\eta})_{ij} = \frac{\partial \dot{\xi}_i}{\partial \eta_j}$, and, $(N_{\xi})_{ij} = \frac{\partial \dot{\eta}_i}{\partial \xi_j}$. We choose $\psi = 0$ without loss of generality.

The equilibrium points are $(\xi_i, \eta_i) = (c_1 + \pi, c_2 + \pi)$. Hence, we can write,

$$(Z_{\xi})_{ij} = \left(\frac{J}{2} + \frac{K}{4} \right) \mathbf{A}_0 - \frac{K}{4} \cos(c_1 - c_2) \mathbf{A}_1, \quad (17)$$

$$(N_{\eta})_{ij} = \left(\frac{J}{2} + \frac{K}{4} \right) \mathbf{A}_0 - \frac{K}{4} \cos(c_1 - c_2) \mathbf{A}_1, \quad (18)$$

$$(Z_{\eta})_{ij} = \left(\frac{J}{2} - \frac{K}{4} \right) \mathbf{A}_0 + \frac{K}{4} \cos(c_1 - c_2) \mathbf{A}_1, \quad (19)$$

$$(N_{\xi})_{ij} = \left(\frac{J}{2} - \frac{K}{4} \right) \mathbf{A}_0 + \frac{K}{4} \cos(c_1 - c_2) \mathbf{A}_1, \quad (20)$$

where

$$\mathbf{A}_0 = \begin{bmatrix} -\frac{N-1}{N} & \frac{1}{N} & \dots & \frac{1}{N} \\ \frac{1}{N} & -\frac{N-1}{N} & \dots & \frac{1}{N} \\ \dots & \dots & \dots & \dots \\ \frac{1}{N} & \dots & \dots & -\frac{N-1}{N} \end{bmatrix}_{N \times N}, \quad (21)$$

and

$$\mathbf{A}_1 = \begin{bmatrix} \frac{N+1}{N} & \frac{1}{N} & \dots & \frac{1}{N} \\ \frac{1}{N} & \frac{N+1}{N} & \dots & \frac{1}{N} \\ \dots & \dots & \dots & \dots \\ \frac{1}{N} & \dots & \dots & \frac{N+1}{N} \end{bmatrix}_{N \times N}. \quad (22)$$

For this state, $c_1 - c_2 = 2\theta_i = 0, 2\pi, 4\pi$. Note that, $M_{s\pi}$ has a dimension of $2N$ since there are two state variables (ξ, θ) for each of the swarmalators and $\dim(A_0) = \dim(A_1) = N$ as both of them are the subblocks of M . Therefore,

$$M_{s\pi} = \begin{bmatrix} \left(\frac{J}{2} + \frac{K}{4} \right) \mathbf{A}_0 - \frac{K}{4} \mathbf{A}_1 & \left(\frac{J}{2} - \frac{K}{4} \right) \mathbf{A}_0 + \frac{K}{4} \mathbf{A}_1 \\ \left(\frac{J}{2} - \frac{K}{4} \right) \mathbf{A}_0 + \frac{K}{4} \mathbf{A}_1 & \left(\frac{J}{2} + \frac{K}{4} \right) \mathbf{A}_0 - \frac{K}{4} \mathbf{A}_1 \end{bmatrix}. \quad (23)$$

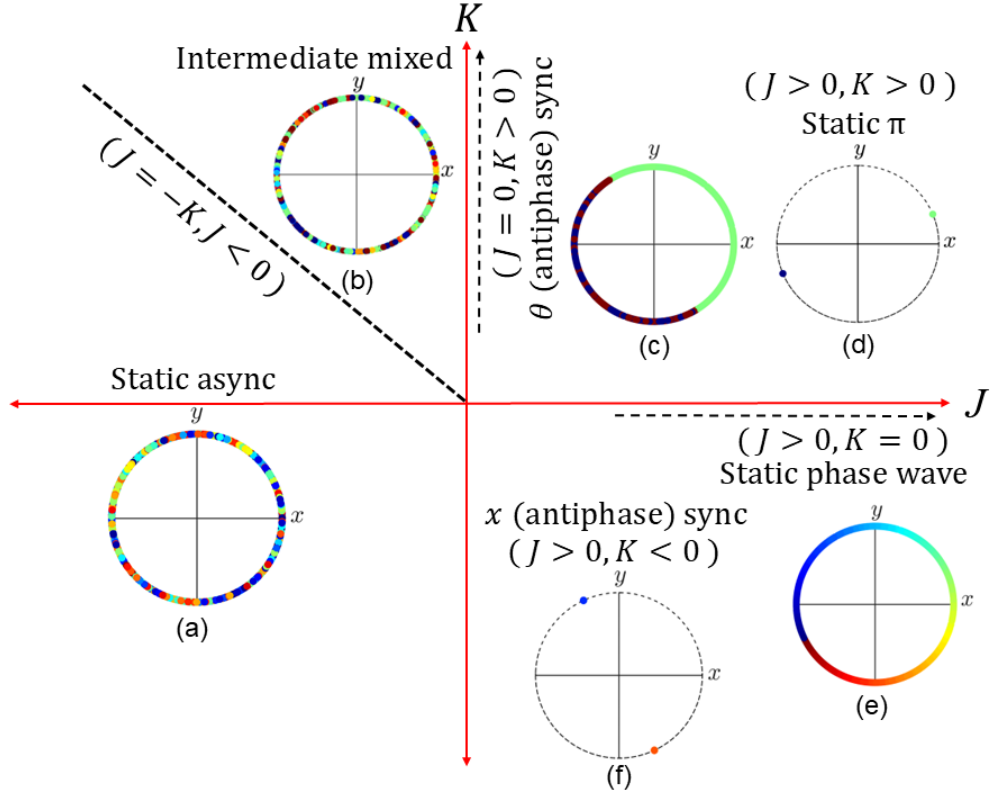


FIG. 1. Schematic diagram of the regions for the states for identical swarmalators. (a) Async: $(J, K) = (-0.5, -0.5)$, (b) intermediate mixed state: $(J, K) = (-0.28, 0.72)$, (c) θ antiphase sync: $(J, K) = (0.0, 0.5)$, (d) static π : $(J, K) = (0.5, 0.5)$, (e) static phase wave: $(J, K) = (0.5, 0.0)$, and (f) x antiphase: $(J, K) = (0.5, -0.5)$. We run the simulations using Heun's method for $N = 1000$ number of swarmalators for $T = 5000$ time units with step-size $dt = 0.1$. Initial positions and phases of the swarmalators are randomly drawn from $[-\pi, \pi]$. All the states are achieved after discarding the first 90% data.

One of the eigenvalues of the matrix \mathbf{A}_0 is $\hat{\lambda} = 0$ due to its rotational symmetry and $(N-1)\hat{\lambda} = -1$. Similarly, for \mathbf{A}_1 , the eigenvalues are 0 and 1 with multiplicity 1 and $(N-1)$.

For any symmetric matrix $E = \begin{pmatrix} C & D \\ D & C \end{pmatrix}$, $\det(E) = \det(C + D)\det(C - D)$. This implies $\det(M_{s\pi}) = \det(J\mathbf{A}_0)\det(\frac{K}{2}(\mathbf{A}_0 - \mathbf{A}_1)) = \det(J\mathbf{A}_0)\det(-K\mathbf{I})$.

As a result the eigenvalues of $M_{s\pi}$ become

$$\lambda = \begin{cases} 0, & \text{multiplicity } 1 \\ -J, & \text{multiplicity } N-1 \\ -K, & \text{multiplicity } N \end{cases} \quad (24)$$

It concludes that the static π state will be stable if $J > 0$ and $K > 0$, which matches our numerics.

2. Stability of the static phase wave state

The calculation for the stability analysis of this state is the same as before. Firstly, we linearize around the

fixed points in the (ξ, η) plane and then find the eigenvalues of the Jacobian matrix M_{spw} . Here, $x_i = 2\pi i/N = \theta_i$ (for $(S_+, S_-) = (1, 0)$ type of phase wave, for $x_i = -\theta_i$, the analysis remains similar). Importantly, this state only exists when $K = 0$; it is not a valid fixed point for $K \neq 0$. So we set $K = 0$ for our analysis, and seek a stability region defined by the parameter J (numerics suggest this is $J > 0$).

The matrix M_{spw} is written as

$$M_{spw} = \begin{bmatrix} Z_\xi & Z_\eta \\ N_\eta & N_\eta \end{bmatrix}_{2N \times 2N} \quad (25)$$

$$\text{Now, } C_{ij} = \cos \frac{2\pi(i-j)}{N}, S_{ij} = \sin \frac{2\pi(i-j)}{N}, \beta_{ij} = C_{ij} + \iota S_{ij}, C_i = \cos \frac{2\pi i}{N}, S_i = \sin \frac{2\pi i}{N}.$$

$$\begin{aligned} \text{Therefore, } \frac{1}{N} \sum_{\substack{j=1 \\ j \neq i}}^N C_{ij} &= \frac{1}{N} \sum_{k=1}^{N-1} C_k \\ &= \frac{1}{N} \left(\sum_{k=0}^{N-1} C_k - C_0 \right) = -\frac{C_0}{N}, \end{aligned} \quad (26)$$

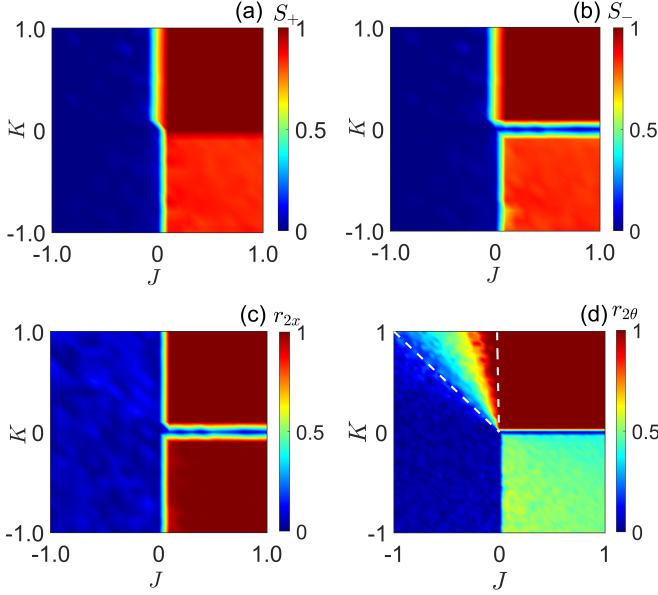


FIG. 2. phase space diagram of the order parameters in the (J, K) plane demonstrating the regions of the collective states. (a) S_+ , (b) S_- , (c) R_{2x} , and (d) $R_{2\theta}$. We simultaneously vary J and K over the interval $[-1.0, 1.0]$. Simulation parameters are $(dt, T, N) = (0.1, 5000, 10^3)$. [We will provide a detailed explanation of Figure (d) in Section III B 5].

where $C_0 = C_{0,0} = 1$. The elements of the matrix M_{spw} are as follows,

$$\begin{aligned}
(Z_\xi)_{ii} &= -\frac{K}{2}r_x \cos \xi_i - \frac{1}{N} \left(\frac{J}{2} + \frac{K}{4} \right) \sum_{j \neq i} \cos(\xi_j - \xi_i) \\
&\quad - \frac{K}{4N} \left(\sum_{\substack{j=1 \\ j \neq i}}^N \cos(\eta_j - \xi_i) + \cos(\eta_i - \xi_i) \right) \\
&= -\frac{1}{N} \left(\frac{J}{2} + \frac{K}{4} \right) \sum_j C_{ij} - C_i \left(\frac{K(N+1)}{4N} - \frac{K}{2}r_x \right) \\
&= \left(\frac{J}{2} + \frac{K}{4} \right) \frac{C_0}{N} - \frac{K}{4} \frac{(N+1)C_i}{N} - \frac{K}{2}r_x C_i, \\
(Z_\xi)_{ij} &= \frac{1}{N} \left(\frac{J}{2} + \frac{K}{4} \right) \cos(\xi_j - \xi_i) - \frac{K}{4N} \cos(\xi_j - \eta_i) \\
&= \left(\frac{J}{2} + \frac{K}{4} \right) \frac{C_{ij}}{N} - \frac{K}{4} \frac{C_i}{N}
\end{aligned}$$

implies, $Z_\xi = \left(\frac{J}{2} + \frac{K}{4} \right) \mathbf{A}_2 - \frac{K}{4} C_i \mathbf{A}_1 - \frac{K}{2} r_x C_i \mathbf{I}$. (27)

By similar calculation, we obtain the other elements as $Z_\eta = \left(\frac{J}{2} - \frac{K}{4} \right) \mathbf{A}_0 + \frac{K}{4} C_i \mathbf{A}_3 + \frac{K}{2} r_x \mathbf{I}$, $N_\xi = \left(\frac{J}{2} - \frac{K}{4} \right) \mathbf{A}_2 + \frac{K}{4} C_i \mathbf{A}_1 + \frac{K}{2} r_x C_i \mathbf{I}$, and $N_\eta = \left(\frac{J}{2} + \frac{K}{4} \right) \mathbf{A}_0 -$

$$\frac{K}{4} C_i \mathbf{A}_3 - \frac{K}{2} r_x \mathbf{I}, \text{ where } A_2 = \begin{bmatrix} \frac{C_0}{N} & \frac{C_{ij}}{N} & \dots & \frac{C_{ij}}{N} \\ \frac{C_{ij}}{N} & \frac{C_0}{N} & \dots & \frac{C_{ij}}{N} \\ \dots & \dots & \dots & \dots \\ \frac{C_{ij}}{N} & \dots & \dots & \frac{C_0}{N} \end{bmatrix} \text{ and}$$

TABLE I. This table highlights the eigenvalues of the Jacobian and their multiplicities for the static phase wave state for different system sizes.

N value	(Eigenvalue, Multiplicity)
2	(0, 4)
3	$(0, 4), \left(-\frac{J}{4}, 2\right)$
4	$(0, 6), \left(-\frac{J}{2}, 2\right)$
$N \geq 5$	$(0, N+1), \left(-\frac{J}{2}, N-3\right), \left(-\frac{J}{4}, 2\right)$

$$A_3 = \begin{bmatrix} \frac{1}{N} & \frac{1}{N} & \dots & \frac{1}{N} \\ \frac{1}{N} & \frac{1}{N} & \dots & \frac{1}{N} \\ \dots & \dots & \dots & \dots \\ \frac{1}{N} & \dots & \dots & \frac{1}{N} \end{bmatrix}.$$

Hence, we can write,

$$\begin{aligned}
M_{spw} &= \begin{bmatrix} J_+ \mathbf{A}_2 & J_- \mathbf{A}_0 \\ J_- \mathbf{A}_2 & J_+ \mathbf{A}_0 \end{bmatrix} + \frac{K}{4} C_i \begin{bmatrix} -\mathbf{A}_1 & \mathbf{A}_3 \\ \mathbf{A}_1 & -\mathbf{A}_3 \end{bmatrix} \\
&\quad + \frac{K}{2} r_x \begin{bmatrix} -C_i & \mathbf{I} \\ C_i & -\mathbf{I} \end{bmatrix}, \tag{28}
\end{aligned}$$

where $J_\pm = \frac{J}{2} \pm \frac{K}{4}$. The matrix has the same structure as M_{spw} for the regular 1d swarmalator model (with Kuramoto type coupling), whose eigenvalues have been computed exactly [23]. A direct extension of this analysis provides the eigenvalues for this case. Table I summarizes these. The cases $N \leq 4$ are special, while a general pattern holds for $N > 4$. In each case, the stability region is $J > 0$, consistent with numerics.

3. Stability of the static async state

We can analyze the stability of this state by going to the continuum limit. Let $\rho(x, \theta, t)$ denote the fraction of swarmalators with positions/phases between $x, x+dx$ and $\theta, \theta+d\theta$ at time t . This density obeys the continuity equation

$$\dot{\rho} + \nabla(v\rho) = 0, \tag{29}$$

where the velocity $v = (v_x, v_\theta)$ is given by

$$\begin{aligned}
v_x &= J \int \sin(x' - x) \cos(\theta' - \theta) \rho(x', \theta', t) dx' d\theta', \\
v_\theta &= K \int \sin \theta (1 + \cos \theta') \cos(x' - x) \rho(x', \theta', t) dx' d\theta'. \tag{30}
\end{aligned}$$

In the limit $N \rightarrow \infty$, the density in the static async state is $\rho_0 = 1/(4\pi^2)$ [49]. We consider a small perturbation around this state such that

$$\rho = \rho_0 + \epsilon \gamma(x, \theta, t). \tag{31}$$

The normalization condition requires $\int \rho(x, \theta, t) dx d\theta = 1$ and therefore we have,

$$\int \gamma(x, \theta, t) dx d\theta = 0. \quad (32)$$

The velocity can be written as,

$$v = v_0 + \epsilon v_1, \quad (33)$$

where v_0 is the velocity in the static async state, which is zero, and we have $v = \epsilon v_1$, where $v_1(v_1^x, v_1^\theta)$ is the perturbed velocity and is given by,

$$\begin{aligned} v_1^x &= \frac{J}{2} \text{Im} \left(W_+^1 e^{-\iota(x+\theta)} + W_-^1 e^{-\iota(x-\theta)} \right), \\ v_1^\theta &= -\frac{K}{4} \text{Im} \left(W_+^1 e^{-\iota(x-\theta)} - W_+^1 e^{-\iota(x+\theta)} + W_-^1 e^{-\iota(x-\theta)} \right. \\ &\quad \left. - W_-^1 e^{-\iota(x+\theta)} + 2R_x^1 e^{-\iota(x-\theta)} - 2R_x^1 e^{-\iota(x+\theta)} \right). \end{aligned} \quad (34)$$

and W_\pm^1 and R_x^1 are the perturbed order parameters and are defined as,

$$W_\pm^1 = \int e^{\iota(x' \pm \theta')} \gamma(x', \theta') dx' d\theta'. \quad (36)$$

Plugging Eq. (31) and Eq. (33) in Eq. (29) obtains

$$\dot{\gamma} + \rho_0(\nabla v_1) = 0, \quad (37)$$

where $\nabla v_1 = \partial_x v_1^x + \partial_\theta v_1^\theta$.

We can calculate ∇v_1 by determining $\partial_x v_1^x$ and $\partial_\theta v_1^\theta$ as,

$$\begin{aligned} \partial_x v_1^x &= -\frac{J}{2} \text{Re} \left[W_+^1 e^{-\iota(x+\theta)} + W_-^1 e^{-\iota(x-\theta)} \right], \\ \partial_x v_1^\theta &= -\frac{K}{4} \text{Re} \left[W_+^1 e^{-\iota(x-\theta)} + W_+^1 e^{-\iota(x+\theta)} + W_-^1 e^{-\iota(x-\theta)} \right. \\ &\quad \left. + W_-^1 e^{-\iota(x+\theta)} + 2R_x^1 e^{-\iota(x-\theta)} + 2R_x^1 e^{-\iota(x+\theta)} \right]. \end{aligned} \quad (38)$$

Therefore, we obtain the time evolution of γ as,

$$\begin{aligned} \dot{\gamma}(x, \theta, t) &= \frac{(2J+K)}{16\pi^2} \text{Re} \left[W_+^1 e^{-\iota(x+\theta)} + W_-^1 e^{-\iota(x-\theta)} \right] \\ &\quad + \frac{K}{16\pi^2} \text{Re} \left[W_+^1 e^{-\iota(x-\theta)} + W_-^1 e^{-\iota(x+\theta)} \right. \\ &\quad \left. + 2R_x^1 e^{-\iota(x-\theta)} + 2R_x^1 e^{-\iota(x+\theta)} \right]. \end{aligned} \quad (39)$$

We expand $\gamma(x, \theta, t)$ in terms of complex exponentials [23] as the following,

$$\begin{aligned} \gamma(x, \theta, t) &= \frac{1}{2\pi} \left(\alpha_{0,0}(t) + \alpha_{1,0}(t) e^{\iota x} + \alpha_{0,1}(t) e^{\iota \theta} \right. \\ &\quad \left. + \sum_{n=1}^{\infty} \sum_{m=1}^{\infty} \tilde{\alpha}_{n,m}(t) e^{\iota(nx+m\theta)} + \tilde{\beta}_{n,m}(t) e^{\iota(nx-m\theta)} + \text{c.c.} \right), \end{aligned} \quad (40)$$

where c.c. denotes complex conjugate. The order parameters are $W_+^1 = \alpha_{1,1}(t)$, $W_-^1 = \beta_{1,1}(t)$, and $R_x^1 = \alpha_{1,0}(t)$. Moreover, due to the normalization condition 32, we have $\alpha_{0,0} = 0$. By projecting onto the Fourier basis, we extract the following evolution equations

$$\dot{W}_\pm^1 = \frac{J}{8\pi} W_\pm^1 + \frac{K}{16\pi} (W_+^1 + W_-^1 + 2R_x^1), \quad (41)$$

$$\dot{R}_x^1 = 0. \quad (42)$$

This is a (linear) three-dimensional dynamic system in the coordinates W_+^1, W_-^1 , and R_x^1 . Therefore, the Jacobian is

$$M_{async} = \begin{pmatrix} \frac{J}{8\pi} + \frac{K}{16\pi} & \frac{K}{16\pi} & \frac{K}{8\pi} \\ \frac{K}{16\pi} & \frac{J}{8\pi} + \frac{K}{16\pi} & \frac{K}{8\pi} \\ 0 & 0 & 0 \end{pmatrix}.$$

The eigenvalues of M_{async} are $\lambda = 0, \frac{J}{8\pi}$ and $\frac{J+K}{8\pi}$. These imply a stability region of

$$\begin{aligned} J &< 0, \\ K &< -J \end{aligned} \quad (43)$$

consistent with numerics. We draw this stability threshold in Fig. 2(d) by the white dashed lines.

4. x (antiphase) sync state

This state is quite difficult to analyze. Look at the scatter plots of the swarmalators in Fig. 3(a). The spatial dynamics are straightforward: there are two equilibrium points shifted π units apart, $x_i = C$ and $C + \pi$ (as evident from the position distribution shown in Fig. 3(b)). We can set the constant $C = 0$ with a change of frame. But the phase equilibrium points are hard to identify. Figure 3(c) shows that the θ_i^* are distributed in two bell-shaped curves, with populations $p, q := 1 - p$, respectively. In general, $p \neq q$, the exact values vary from run to run.

To try and find these equilibrium points, we write the phase equation (Eq. 4) in the continuum limit,

$$v_\theta = -\sin \theta \int (1 + \cos \theta') \cos(x' - x) \rho(x', \theta') dx' d\theta', \quad (44)$$

where the density of the state is $\rho(x, \theta) = p\delta(x)P_p(\theta) + q\delta(x - \pi)P_q(\theta)$. Here $P_{p,q}(\theta)$ denotes the densities of the two sub-populations. In this notation, the phase velocity becomes

$$\begin{aligned} v_\theta &= -\sin \theta \left[p \cos x \int_{\pi}^{2\pi} (1 + \cos \theta') P_p(\theta') d\theta' \right. \\ &\quad \left. + q \cos(\pi - x) \int_0^{\pi} (1 + \cos \theta') P_q(\theta') d\theta' \right], \end{aligned} \quad (45)$$

which implies

$$v_\theta = -\sin\theta \cos x \left[p(1 + I_p) - q(1 + I_q) \right], \quad (46)$$

where $I_{p,q} = \int P_{p,q}(\theta) d\theta$ denote the definite integrals of $P_{p,q}(\theta)$ over their domain. Now, we know $v_\theta = 0$ at $x = 0$ and π , which means the term within the brackets must be zero, i.e.,

$$p(1 + I_p) - q(1 + I_q) = 0, \quad (47)$$

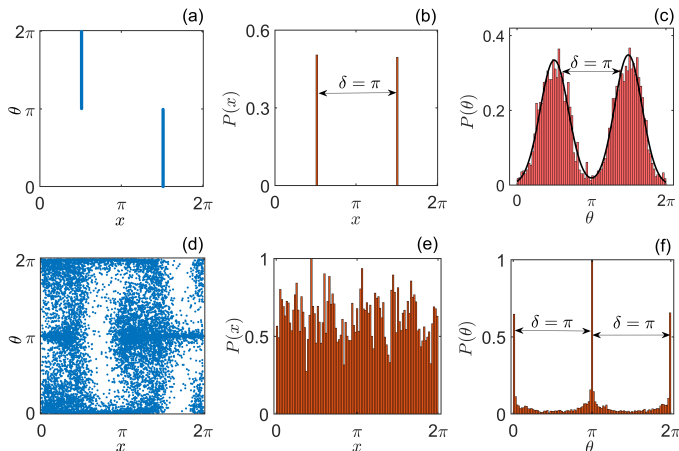


FIG. 3. (a) Scatter plot of the x (antiphase) sync state $[(J, K) = (0.5, -0.5)]$ in (x, θ) plane, (b) & (c) denote the distribution of x and θ in the x (antiphase) sync state. (d) Scatter plot of the intermediate mixed state $[(J, K) = (-0.28, 0.76)]$ in (x, θ) plane, (e) & (f) depict the corresponding distribution of x and θ . The simulation parameters are $(dt, T, N) = (0.1, 5000, 10^4)$.

where we have requoted the definition of $I_{p,q}$ for convenience. Eq. (47) is the equilibrium point condition for this state. Any phase density $P_{p,q}(\theta)$ that satisfies the above is a solution. We have confirmed Eq. (47) numerically by calculating $(p, q), (I_p, I_q)$ for different population sizes N , depicted in Fig. 4.

Now, getting back to an analytic perspective, what are the equilibrium densities $P_{p,q}(\theta)$ that satisfy Eq. (47)? There is an infinite number. Yet numerics suggest only one of these is stable, the bell-shaped distributions in Figure 3(c), which are well fit by a wrapped Gaussian (thick black lines in panel (c)). We are unable to make any headway on proving this analytically. The formal approach would be to linearize around the equilibrium density

$$\rho_0(x, \theta) = p\delta(x)P_p(\theta) + q\delta(x - \pi)P_q(\theta) \quad (48)$$

with $P_{p,q}(\theta)$ wrapped Gaussians, in the same way we linearized around the async density $\rho_0 = (4\pi^2)^{-1}$. However, the presence of $\delta(x)$ functions and the wrapped Gaussian makes the calculation significantly more complex and beyond the scope of this paper.

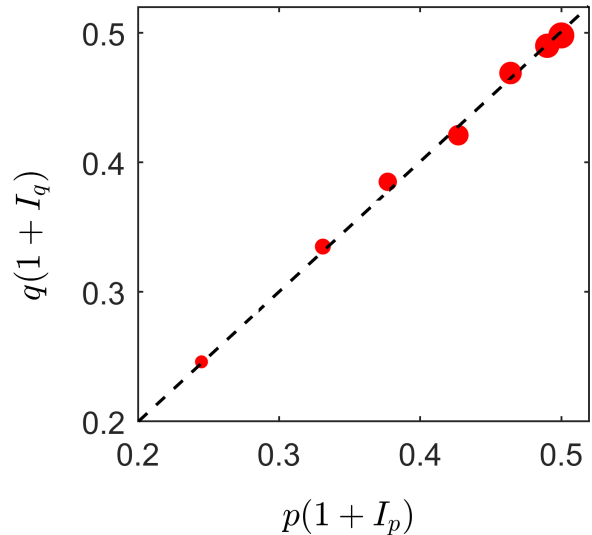


FIG. 4. The black dashed line represents the prediction of Eq. (47); For numerical validation, we simulate the system for $N = 2, 3, 4, 5, 20, 50, 100$ number of particles (as indicated by increasing the size of the red dots), which closely align with our analytical results. Simulation parameters $(dt, T, J, K) = (0.1, 5 \times 10^4, 0.5, -0.5)$. After wiping out the transients, we save the last 10% data by taking 100 realizations.

5. Intermediate mixed state

This state appears in the range between $J = 0$ and $J = -K \forall J < 0$ in Fig. 2(d). Figure 3(d) depicts the scatter plot of the swarmalators in the (x, θ) plane. Here, the particles are positionally asynchronous. However, a detailed examination of their phases reveals that while some form clusters with a phase difference of approximately π , the others remain randomly distributed (notice the distribution of positions and phases in Fig. 3(e) and (f) respectively). We term this the intermediate mixed state, where swarmalators are neither fully antiphase nor entirely asynchronous.

Interestingly, the swarmalators exhibit slight oscillations and eventually shift their positions slowly over time. This slow behavior is somewhat reminiscent of glassy phenomena. Figure 5 investigates this slow relaxation by plotting the mean velocity $\langle v \rangle (= \sqrt{\Delta x^2 + \Delta \theta^2})$ of the system over time. Panels (a) and (b) of Fig. 5 illustrate that for small system sizes ($N = 3, 5$), the system gets gradually cooler and eventually freezes at 10^5 steps. In contrast, panels (c) and (d) of Fig. 5 show that for larger system sizes ($N = 50, 200$), although the system gradually cools as before, it never appears to freeze fully. Instead, finite fluctuations in $\langle v \rangle$ appear to persist indefinitely. We ran simulations for up to 10^7 steps and never saw the motion die out. To distinguish this state, we examine the order parameters $r_{x(\theta)}$ (see Fig. 6(a) and (b))

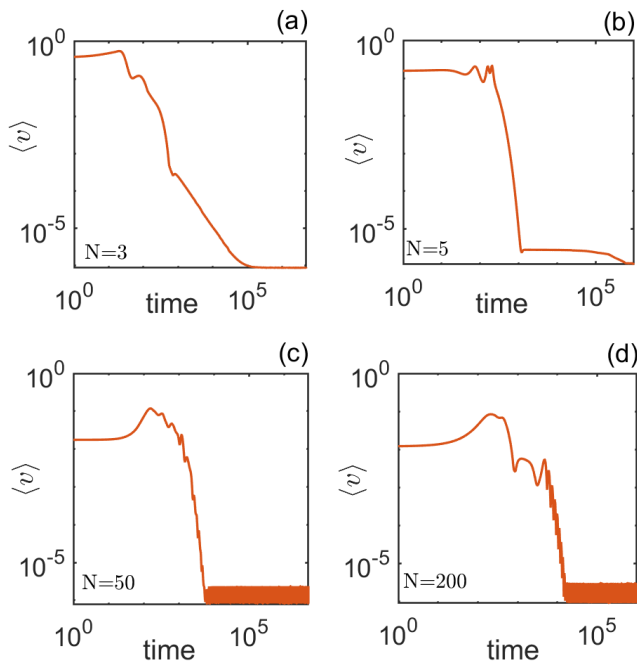


FIG. 5. A log-log plot of the time evolution of mean velocity $\langle v \rangle$ of the swarmalators at different values of N for intermediate mixed state. We set $(J, K) = (-0.28, 0.76)$.

and $r_{2x(\theta)}$ (notice Fig. 6(c) and 6(d)) over J for various K . We observe that all the order parameters behave the same at distinct K except $r_{2\theta}$. For larger values of K , $r_{2\theta}$ increases and approaches unity.

6. θ (antiphase) sync state

This state arises exclusively for the special case $J = 0$, where spatial dynamics are inactive. As a result, the spatial configuration remains as initially set, uniformly random. See Fig. 7(a), where we plot the positions of the swarmalators according to their indices. Rather, they exhibit a phase separation of π (look at Fig. 7(b)). We can find the stability of this state via standard, finite- N linearization (we take $x_i = \frac{2\pi i}{N}$ linearly spaced and $\theta_i = \pi\Theta(i - (\frac{N}{2} + 1))$, where $\Theta(\cdot)$ is the Heaviside function). The eigenvalues for this state are as indicated in Table II, where C_i are the positive constants that depend on N . This corroborates our numerical findings that the state is stable if $K > 0$ when it exists for $J = 0$.

IV. CONCLUSION

Our contribution is the first study of swarmalators with Winfree-type coupling, where the elements fire pulses according to a function $P(\theta)$ received by the other elements via a response function $R(\theta)$. This type of cou-

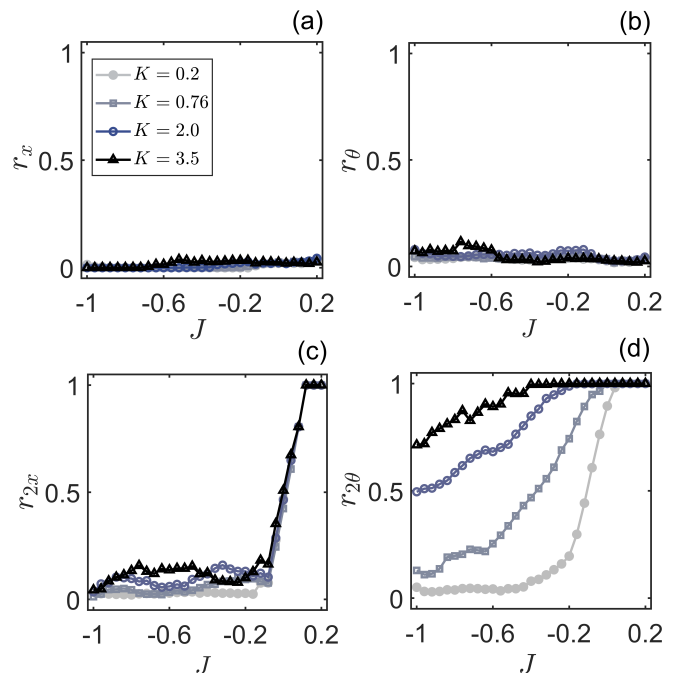


FIG. 6. Variation of $r_{x(\theta)}$ and $r_{2x(\theta)}$ with J for distinct values of K . We codify the system for $(dt, T, N) = (0.1, 5000, 10^3)$ and calculate the order parameters after wiping out the first 90% data.

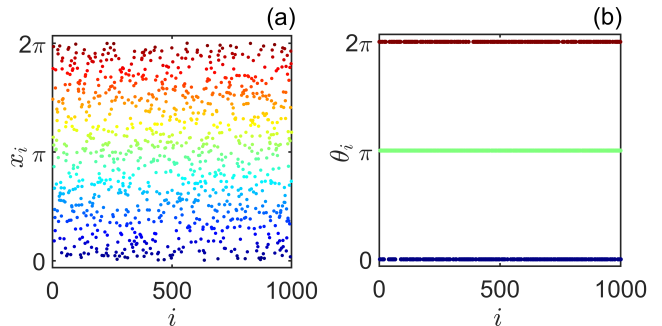


FIG. 7. θ (antiphase) sync state for $(J, K) = (0.0, 0.5)$. (a) The position of the swarmalators is plotted (colors representing their positions) against their indices. (b) Scatter plot of the swarmalators' phase concerning their index (colored according to their phases), Simulation parameters are $(dt, T, N) = (0.1, 5000, 10^3)$. Initially, both their phases and positions are randomly chosen from $[-\pi, \pi]$.

pling is observed in many systems, such as fireflies or neurons, and in some sense generalizes the Kuramoto-type coupling. Table III shows that Winfree coupling recovers the states seen with Kuramoto coupling (static π , phase wave, and async states) but also produces three new collective states (x, θ -antiphase sync states and the intermediate mixed state). On the other hand, the active async state that appears with Kuramoto-type coupling was not observed.

TABLE II. This table demonstrates the eigenvalues and multiplicity of the Jacobian for the θ (antiphase) sync state at distinct system sizes.

N value	(Eigenvalue, Multiplicity)
2	$(0, 2), (-K, 2)$
3	$(0, 3), (-\frac{2K}{3}, 1), (\frac{K}{3}, 2)$
4	$(0, 4), (-\frac{K}{2}, 4)$
6	$(0, 6), (-\frac{2K}{3}, 2), (-\frac{K}{3}, 4)$
8	$(0, 8), (-\frac{K}{4}, 4), (-\frac{(1+\sqrt{2})K}{4}, 4)$
N	$(0, N), (-C_i(N)K, N)$

We determined the stability thresholds for four of these six states; the stability of the mixed and x -antiphase sync state remain out of reach. A natural question for follow-up work is to try and pin these down. Take the antiphase state. As discussed, its properties are somewhat unusual: an infinite number of equilibrium densities P_θ satisfy the state, yet only one, the bell-

shaped distribution well fit by a Gaussian, appears to be stable. Why is that? Why is it fit so well by a Gaussian? And is it truly the only stable equilibrium, or could others exist that the numerics failed to reveal?

Future work could also relax some of the idealizations we made in the work. For instance, one could on the natural frequencies (ω_i, ν_i) or draw them from some distribution. Heterogeneities in the coupling constants would also be interesting to investigate.

TABLE III. Comparison of the emerging states in 1d swarms between the Kuramoto coupling and the Winfree coupling:

State	Kuramoto coupling	Winfree coupling
Static π	✓	✓
Static async	✓	✓
Static phase wave	✓	✓
Active async	✓	×
x -(antiphase) sync	×	✓
θ -(antiphase) sync	×	✓
Intermediate mixed	×	✓

- [1] A. T. Winfree, *The geometry of biological time*, vol. 2 (Springer, 1980).
- [2] M. Rosenblum and J. Kurths, *Synchronization: a universal concept in nonlinear science* (Cambridge University Press, 2003).
- [3] L. M. Pecora and T. L. Carroll, Physical Review Letters **64**, 821 (1990).
- [4] S. Boccaletti, J. Kurths, G. Osipov, D. Valladares, and C. Zhou, Physics Reports **366**, 1 (2002).
- [5] S. Pal, G. K. Sar, D. Ghosh, and A. Pal, Chaos **34**, 021103 (2024).
- [6] W. Bialek, A. Cavagna, I. Giardina, T. Mora, E. Silvestri, M. Viale, and A. M. Walczak, Proceedings of the National Academy of Sciences **109**, 4786 (2012).
- [7] R. C. Fetecau, Y. Huang, and T. Kolokolnikov, Nonlinearity **24**, 2681 (2011).
- [8] N. C. Darnton, L. Turner, S. Rojevsky, and H. C. Berg, Biophysical Journal **98**, 2082 (2010).
- [9] A. Mogilner and L. Edelstein-Keshet, Journal of Mathematical Biology **38**, 534 (1999).
- [10] I. H. Riedel, K. Kruse, and J. Howard, Science **309**, 300 (2005).
- [11] A. Quillen, A. Peshkov, E. Wright, and S. McGaffigan, Physical Review E **104**, 014412 (2021).
- [12] J. Yan, M. Bloom, S. C. Bae, E. Luijten, and S. Granick, Nature **491**, 578 (2012).
- [13] A. Bricard, J.-B. Caussin, D. Das, C. Savoie, V. Chikkadi, K. Shitara, O. Chepizhko, F. Peruani, D. Saintillan, and D. Bartolo, Nature Communications **6**, 7470 (2015).
- [14] A. Hravec, V. Křizáková, S. Pizzini, J. Sampaio, A. Thiville, S. Rohart, and J. Vogel, Physical Review Letters **120**, 227204 (2018).
- [15] A. Barciś and C. Bettstetter, IEEE Access **8**, 218752 (2020).
- [16] M. S. Talamali, A. Saha, J. A. Marshall, and A. Reina, Science Robotics **6**, eabf1416 (2021).
- [17] J. D. Monaco, G. M. Hwang, K. M. Schultz, and K. Zhang, Biological Cybernetics **114**, 269 (2020).
- [18] D. Tanaka, Physical Review Letters **99**, 134103 (2007).
- [19] M. Iwasa, K. Iida, and D. Tanaka, Physical Review E **81**, 046220 (2010).
- [20] M. Iwasa and D. Tanaka, Physical Review E **81**, 066214 (2010).
- [21] K. P. O’Keeffe, H. Hong, and S. H. Strogatz, Nature Communications **8**, 1504 (2017).
- [22] J. U. Lizarraga and M. A. de Aguiar, Chaos **30**, 053112 (2020).
- [23] K. O’Keeffe, S. Ceron, and K. Petersen, Physical Review E **105**, 014211 (2022).
- [24] G. K. Sar, D. Ghosh, and K. O’Keeffe, Physical Review E **107**, 024215 (2023).
- [25] B. Hao, M. Zhong, and K. O’Keeffe, Physical Review E **108**, 064214 (2023).
- [26] S. J. Kongni, V. Nguefoue, T. Njouougou, P. Louodop, F. F. Ferreira, R. Tchitnga, and H. A. Cerdeira, Physical Review E **108**, 034303 (2023).
- [27] H. Hong, K. P. O’Keeffe, J. S. Lee, and H. Park, Physical Review Research **5**, 023105 (2023).
- [28] S. Ghosh, G. K. Sar, S. Majhi, and D. Ghosh, Physical Review E **108**, 034217 (2023).
- [29] X. Xu, Y. Lu, S. Wang, J. Xu, and Z. Zheng, Chaos **34**,

- 113103 (2024).
- [30] S. J. Kongni, T. Njougouo, P. Louodop, R. Tchitnga, F. F. Ferreira, and H. A. Cerdeira, *Physical Review E* **110**, L062301 (2024).
- [31] S. Ghosh, S. Pal, G. K. Sar, and D. Ghosh, *Physical Review E* **109**, 054205 (2024).
- [32] S. Ceron, W. Xiao, and D. Rus, in *2024 IEEE International Conference on Robotics and Automation (ICRA)* (IEEE, 2024), pp. 12233–12239.
- [33] N. Blum, A. Li, K. O’Keeffe, and O. Kogan, *Physical Review E* **109**, 014205 (2024).
- [34] S. Fasciani, P. P. Lucas Bravo, A. Szorkovszky, and K. Glette, in *Proceedings of the International Conference on New Interfaces for Musical Expression* (NIME, 2024).
- [35] J. U. Lizárraga, K. P. O’Keeffe, and M. A. de Aguiar, *Physical Review E* **109**, 044209 (2024).
- [36] L. D. Smith, *SIAM Journal on Applied Dynamical Systems* **23**, 1133 (2024).
- [37] G. K. Sar, M. S. Anwar, M. Moriamé, D. Ghosh, and T. Carletti, *Physical Review E* **111**, 034212 (2025).
- [38] Y. Kuramoto and Y. Kuramoto, *Chemical turbulence* (Springer, 1984).
- [39] K. O’Keeffe, G. K. Sar, M. S. Anwar, J. U. Lizárraga, M. A. de Aguiar, and D. Ghosh, in *Proceedings A* (The Royal Society, 2024), vol. 480, p. 20240448.
- [40] S. Yoon, K. O’Keeffe, J. Mendes, and A. Goltsev, *Physical Review Letters* **129**, 208002 (2022).
- [41] K. O’Keeffe, *Chaos* **35**, 023150 (2025).
- [42] K. O’Keeffe, arXiv preprint arXiv:2410.02975 (2024).
- [43] K. O’Keeffe and H. Hong, *Physical Review E* **105**, 064208 (2022).
- [44] J. U. Lizárraga and M. A. de Aguiar, *Physical Review E* **108**, 024212 (2023).
- [45] G. K. Sar, D. Ghosh, and K. O’Keeffe, *Physical Review E* **109**, 044603 (2024).
- [46] G. K. Sar, K. O’Keeffe, and D. Ghosh, *Chaos* **33**, 111103 (2023).
- [47] M. S. Anwar, D. Ghosh, and K. O’Keeffe, *Physical Review E* **111**, 044207 (2025).
- [48] M. S. Anwar, G. K. Sar, M. Perc, and D. Ghosh, *Communications Physics* **7**, 59 (2024).
- [49] G. K. Sar, K. O’Keeffe, and D. Ghosh, *Physical Review E* **111**, 024206 (2025).
- [50] J. T. Ariaratnam and S. H. Strogatz, *Physical Review Letters* **86**, 4278 (2001).